Isobaric Analog States of Ti^{51} Studied by Elastic and Inelastic Scattering of Protons on Ti^{50}†

E. R. COSMAN, D. C. SLATER, AND J. E. SPENCER
Physics Department and Laboratory for Nuclear Science, Massachusetts Institute of Technology, Cambridge, Massachusetts

(Received 2 October 1968)

The isobaric analogs of levels in Ti^{51} from $E_x=2.0$–5.5 MeV are observed here as resonances in (p, p') scattering on Ti^{50}. Excitation functions for the inelastic $p_1'(2^+)$ and $p_2'(4^+)$ transitions have been determined at $\theta_{lab}=90°$ and 160° from an incident energy of 3.4–7.1 MeV. Twenty-two analog resonances have been identified within this range, and aspects of the accompanying intermediate and fine structure are discussed. Several on-resonance angular distributions have been measured. In some cases, they display marked asymmetries about 90°, indicating the presence of direct-reaction interference effects. A Breit-Wigner analysis of the elastic and inelastic data was carried out, and the resulting partial and total widths are given. The associated spectroscopic factors and excitation energies are compared with the values found from $Ti^{50}(d, p)Ti^{51}$. Several possible reaction processes are considered in the description of the resonant inelastic proton transitions to the first 0^+, 3^+, and 4^+ states in Ti^{50}, and information on the levels of Ti^{51} is discussed in terms of the core-excited model.

I. INTRODUCTION

THERE is evidence[1] that Ti^{50} has a nearly pure $(f_{7/2})_n^8$ neutron configuration closing the major shell at $N=28$. Furthermore, it appears[1,2] that the lowest four levels below 3.2-MeV excitation in Ti^{50} with $J^\pi=0^+$, 2^+, 4^+, and 6^+ are well described as $(f_{7/2})_p^2$ proton configurations and that neutron particle-hole states begin appearing only above 4 MeV. A reasonable picture for the lowest-lying levels in Ti^{51} might then be the core-excited model[3] in which they are constructed by coupling single neutrons in orbits above the $f_{7/2}$ shell to these lowest-excited states in the neighboring Ti^{50} system. To first order, the multiplets of levels thus formed should have centroid excitation energies equal to the sum of those for the particle states in Ti^{51} and core states in Ti^{50}, and should possess many of the properties of the latter. Configurations built on different excited-core states may mix if they have the same spin and parity and are close enough in excitation energy; this is a probable explanation of the observed fragmentation of the single-neutron strength (neutron plus Ti^{50} ground state) seen in $Ti^{50}(d, p)Ti^{51}$ (Ref. 2). Some configurations, such as $[(f_{5/2})_n\phi_{2^+}]_{9/2^-}$, have no nearby single-neutron states with which to mix. Candidates for such nonsingle-particle levels have also been identified in $Ti^{50}(d, p)Ti^{51}$ (Ref. 1), where they are populated by weak so-called nonstripping transitions.

In this paper, we study the isobaric analogs of the low-lying levels in Ti^{51} between excitation energies of 2.0 and 5.5 MeV. They exist as narrow virtual levels in V^{51} at excitations from 11.4 to 15.0 MeV in that nucleus and are populated here by resonant elastic and inelastic proton scattering on Ti^{50}. The level schemes and reaction routes considered are illustrated in Fig. 1.

The associated elastic widths are a measure of the single-particle character of the level and thus may be compared with known spectroscopic factors from the $Ti^{50}(d, p)Ti^{51}$ reaction. The inelastic widths and angular distributions, on the other hand, provide information on the overlap between the analog configuration and particles coupled to the excited states of Ti^{50} and are therefore relevant to a core-excited interpretation. However, several difficulties are anticipated in extracting these widths from the data and will be examined here. Perhaps the foremost of these are (a) the dissolution of a well-defined resonance structure in the cross sections for the lighter nuclei where fine modulations caused by mixing of the analog and compound-nucleus states become amplified, and the background fluctuations are increased, and (b) the presence of resonance direct-reaction interference in the inelastic scattering which destroys the symmetry of angular distributions and, therefore, the possibility of making reliable Legendre polynomial fits and spin determinations. This effect[4] has been observed in $Sr^{88}(p, p')$ for transitions to collective states, and it is of interest to see whether it persists here where the lowest states in Ti^{50} are not of a strongly collective character.

II. EXPERIMENTAL METHOD AND RESULTS

Protons from the MIT-ONR Van de Graaff accelerator were used to obtain the elastic and inelastic excitation functions on Ti^{50} from $E_p=3.4$–7.2 MeV. The scattered particles were detected simultaneously at two angles, $\theta_{lab}=90°$ and 160°, with silicon surface-barrier detectors mounted inside the target chamber

† Work supported in part through funds provided by the U.S. Atomic Energy Commission under AEC Contract No. AT(30-1)-2098.

[1] P. D. Barnes, C. K. Bockelman, Ole Hansen, and A. Sperduto, Phys. Rev. **136**, B438 (1964); P. Wilhjelm, Ole Hansen, J. R. Comfort, C. K. Bockelman, P. D. Barnes, and A. Sperduto, *ibid.* **166**, 1121 (1968).

[2] P. D. Barnes, C. K. Bockelman, Ole Hansen, and A. Sperduto, Phys. Rev. **140**, B42 (1965).

[3] A. de-Shalit, Phys. Rev. **122**, 1530 (1961).

[4] E. R. Cosman, J. M. Joyce, and S. M. Shafroth, Nucl. Phys. **A108**, 519 (1968); E. R. Cosman, H. A. Enge, and A. Sperduto, Phys. Letters **22**, 195 (1966).

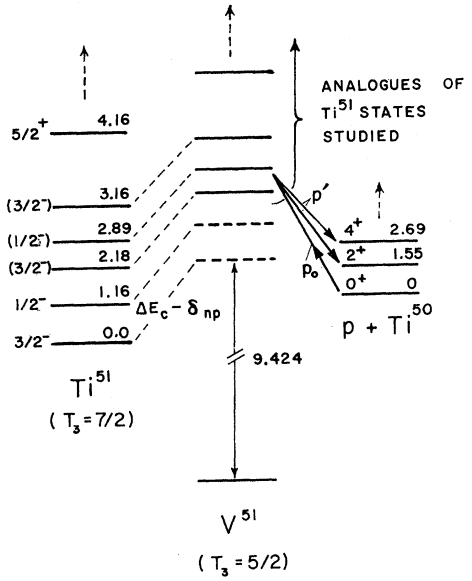

FIG. 1. Level schemes and reaction routes considered in the present experiment. The lowest levels in Ti^{51} are connected by dashed lines to their isobaric analogs in V^{51}. The latter exist as narrow virtual states with $T=\frac{7}{2}$ in a region of high density of $T=\frac{5}{2}$ or normal states. They are populated here by resonant proton capture on a Ti^{50} target, but once formed may decay to the excited states of the Ti^{50} system. We have studied only the analogs of levels from $E_x=2.0$–5.5 MeV in Ti^{51} and report here on resonant transitions of the $Ti^{50}+p$ reaction in the $p_0(0^+)$, $p'_1(2^+)$, and $p'_2(4^+)$ channels.

of the MIT multiple-gap spectrograph.[5] On- and off-resonance angular distributions for the inelastic transitions were measured on nuclear emulsions from $\theta=7.5°$ and 172° with this spectrograph. During the exposures, the drift in the incident beam energy was kept to less than 1 keV by continuous monitoring of the solid-state counter yields and magnetic field settings. The target consisted of a layer of TiO_2 evaporated onto a thin carbon backing. The isotopic composition of the target material was 1.5% Ti^{46}, 1.6% Ti^{47}, 11.9% Ti^{48}, 3.9% Ti^{49}, and 81.5% Ti^{50}, and the thickness of Ti^{50} was 26 $\mu g/cm^2$.

Figures 2 and 3 show the excitation functions obtained for the 0_1^+, 2_1^+, and 4_1^+ transitions with $Q=0.0$, -1.555, and -2.686 MeV, respectively. Over this range of energy, the other Ti^{50} inelastic peaks were either too weak to be seen or were obscured by contaminant groups. A discussion of the details of these figures is given in Sec. III. Several on-resonance inelastic angular distributions were also measured and described in Sec. III C.

III. ANALYSIS AND DISCUSSION

A. Structure in Excitation Functions

The $p_1'(2^+)$ channel shows a large amount of structure that appears to be a strong signature of the analog states seen here. The over-all structure seems to come in three orders illustrated well by the $2p$ anomaly at $E_p=4.3$ MeV (see Fig. 2). (a) First, there is the gross strength function with a typical width from 25 to 100 keV, (b) then, there are the fine-structure fragments within this strength function with widths and spacings of about 15 keV, and (c) finally, there are the small, reproducible fluctuations that cover the entire excitation function and have widths of 5 keV or less.

The spacings of the enhancements of type (a) indicate that they locate the $T_>=\frac{7}{2}$ doorway configurations in V^{51} that are analogs to the parent levels in Ti^{51}. The type (b) fragments probably arise from the underlying $T_<=\frac{5}{2}$ or "normal" states in V^{51} that have the same J^π as the analog level and are admixed with it. Their spacings are roughly consistent with expected density for such states in this region,[6] e.g., 30–100 per MeV with $J^\pi=\frac{1}{2}^-$ or $\frac{3}{2}^-$; however, it may be only a certain subclass of these, such as other $2p$-$1h$ or $3p$-$2h$ configurations, that is primarily responsible for the large fragments seen here.[7] The last order of structure, type (c), should be the incoherent background from all the states of the compound V^{51} system which is estimated[6] to be 25 000 per MeV.

The elastic data show similar structure, but the interference shapes corresponding to type (a) above are generally less obvious, and the background fluctuations of type (c) are relatively more pronounced. The latter fact makes the discrimination of an elastic analog-state anomaly from background almost hopeless in some cases. An example of this is seen in Fig. 2 for the range $E_p=3.5$–4.7 MeV, where deviations from the Rutherford average are as large and narrow off resonance as they are on the region of the strong $2p$-wave analog resonances. We have attempted to wash out artificially the fine structure and reveal the analog states more clearly by averaging the data with a Gaussian weighting function and averaging intervals of $I=20$ and 35 keV. The resulting curve in Fig. 4 is smoother; however, in many cases, such as the p state at $E_p=4.3$ MeV, the analog shape still shows underlying modulations.

A suggested match between the analog resonances seen here and their parent states in Ti^{51} is indicated by the dashed guidelines in Figs. 2 and 3 and listed explicitly in Table I. For the pronounced single-particle states, this correspondence is obvious; however, for other cases, it is more speculative. The $2p$ and $2d$ states [$l=1$ and 2 from (d, p)] are clearly visible and seem to undergo small relative Coulomb energy shifts (see Figs. 2 and 3). We have made a tentative correspondence between the $3s_{1/2}$ analogs and the $p_1'(2^+)$ enhancements seen near their expected positions, al-

[5] H. A. Enge and W. W. Buechner, Rev. Sci. Instr. **34**, 155 (1963).

[6] E. Godioli and L. Zetta, Phys. Rev. **167**, 1016 (1967); A. Gilbert and A. G. W. Cameron, Can. J. Phys. **43**, 1446 (1965).

[7] M. Divadeenam and W. P. Beres, Phys. Rev. Letters **21**, 379 (1968).

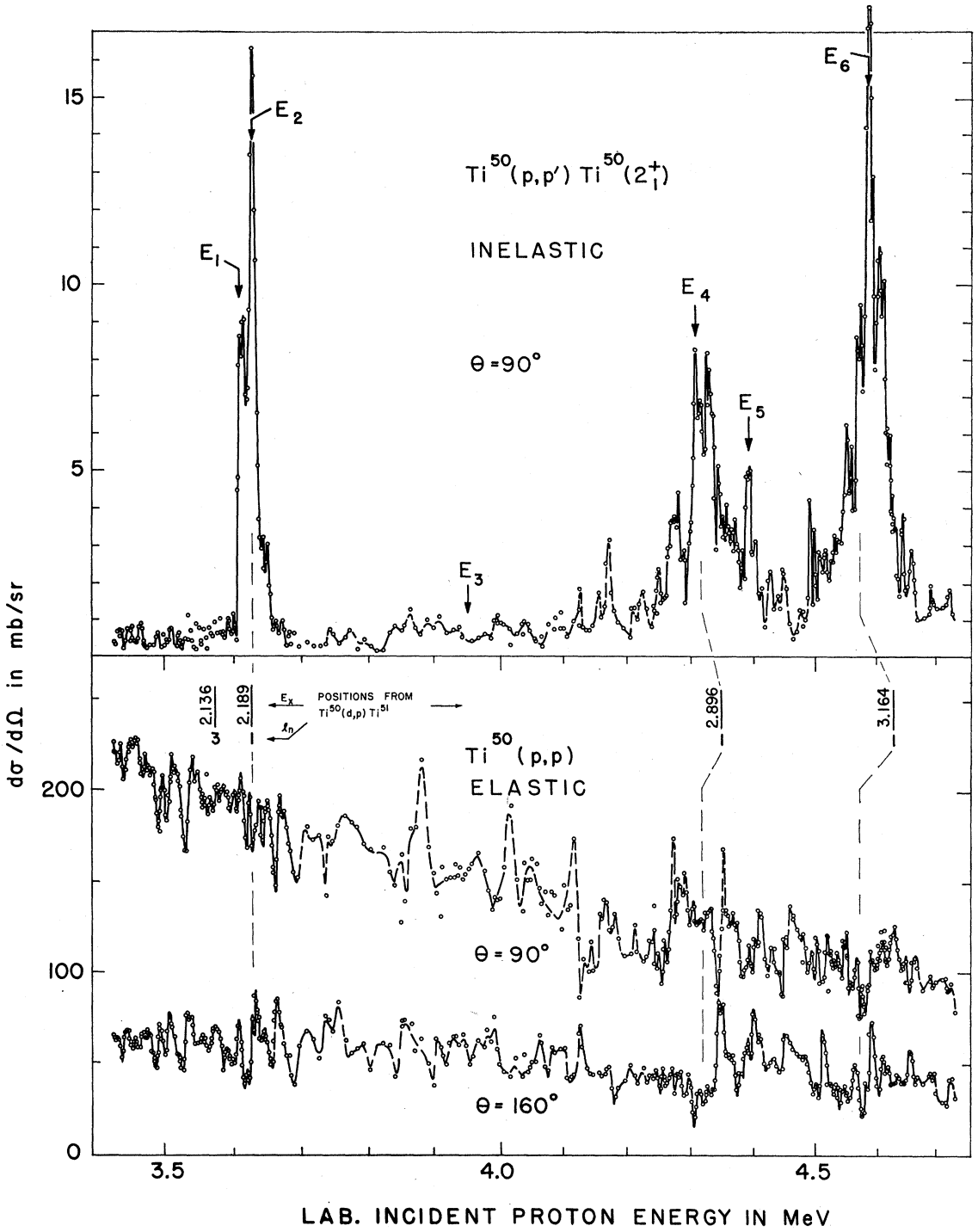

FIG. 2. Excitation functions for $Ti^{50}+p$ taken with solid-state detectors. The upper graph shows the yield at 90° for the inelastic transition to the 2_1^+ state at $E_x=1.555$ MeV in Ti^{50}. The lower graph shows the corresponding elastic data at 90° and 160°. The curves through the data points are hand drawn as a guideline to the resonant shapes. Also shown by the vertical lines are positions expected for analog levels derived from results of the $Ti^{50}(d, p)Ti^{51}$ reaction. See Ref. 1. They are drawn with respect to the lowest $2p_{3/2}$ resonance at $E_p=3.626$ MeV. The dashed vertical guidelines in this and the next figure are intended to suggest a possible matching of Ti^{51} levels to analogs given explicitly in Table I. The arrows above the inelastic excitation function mark the incident energies for which angular distributions were measured in separated exposures using the MIT multiple-gap spectrograph.

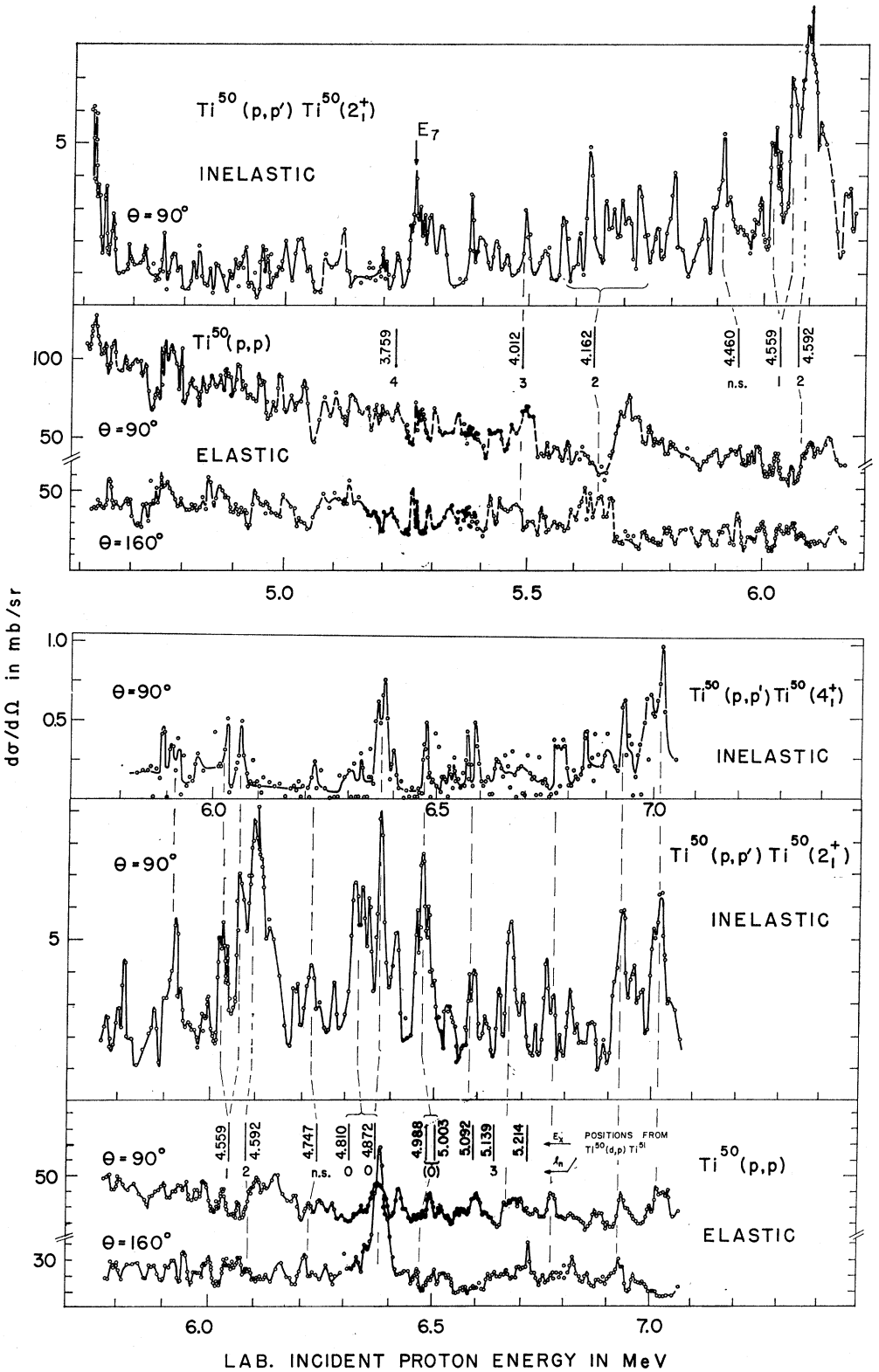

FIG. 3. Excitation functions (continued). This is the extension to higher energies of the data shown in Fig. 1. Also included in the drawing is the yield to the 4_1^+ state at $E_x = 2.686$ MeV in Ti^{50}.

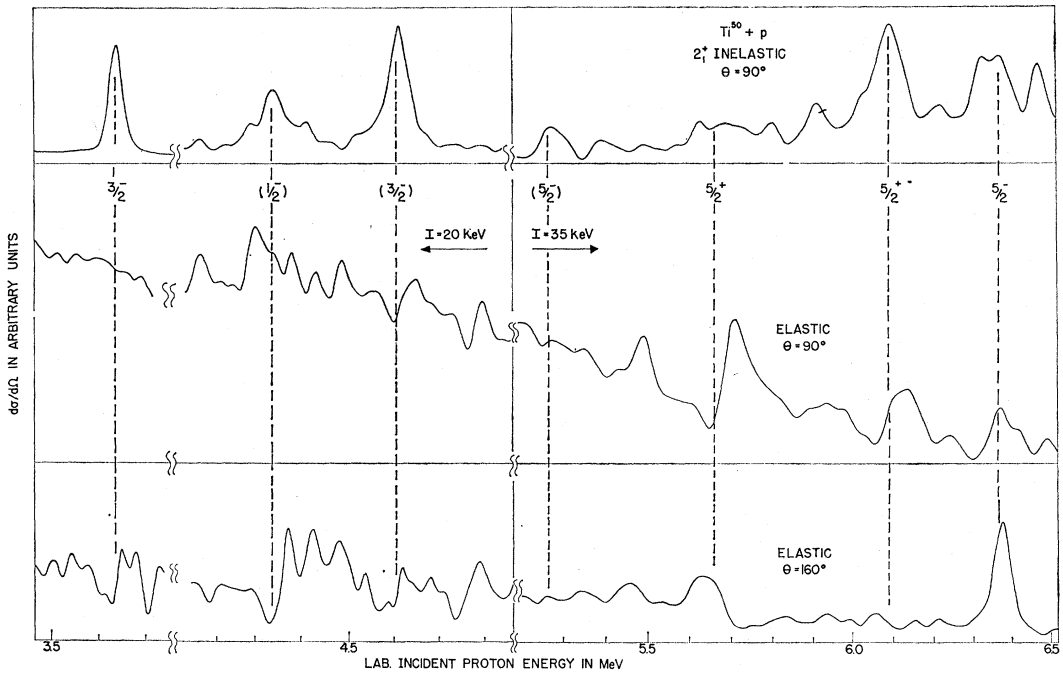

FIG. 4. The curve in this figure was calculated by averaging the solid curve through the data points in Figs. 2 and 3 with a Gaussian weighting function. Averaging intervals of $I=20$ and 35 keV were used in the regions indicated. The cross-section scales for the different segments of the curve vary and are in arbitrary units. The dashed vertical guidelines located the positions of the strongest single-particle analog states seen. Although the corresponding resonance shapes are in general evident here, remnants of the fine structure and fluctuations in the data are also present after averaging, and they obscure the simple patterns in some cases (e.g., the $2p_{3/2}$ elastic resonance at $E_p=3.62$ MeV).

though no recognizable $l=0$ elastic shapes seem to be present at the same locations. This assignment would imply that the $2d$ and $3s$ resonances also are not shifted relative to each other, which is consistent with previous data.[4]

The large elastic anomaly at 6.40 MeV appears to be of f-wave character and corresponds most closely to the analog of the 4.872-MeV state in Ti^{51}. The latter was assigned $l_n=0$ from $Ti^{50}(d, p)Ti^{51}$ in Ref. 4. The appearance of the angular distribution from the stripping is not inconsistent with an $l_n=3$ assignment,[8] and, therefore, our data would favor this assignment. If this is correct, then the assignment of $l_n=3$ in Ref. 4 to the state at $E_x=5.139$ MeV, which has comparable strength to the 4.872-MeV state in the (d, p) study, is also questionable, since we see no corresponding f-wave resonance in our data. However, near the expected position, the elastic cross section does show a pattern that resembles an $l=2$ resonance and might indicate the 5.159-MeV state is of d-wave character. Two other $l=3$ analogs might be expected from the $Ti^{50}(d, p)Ti^{51}$ results, corresponding to the $E_x=2.136$ and 4.012 MeV states in Ti^{51}. No conclusive evidence for such resonances is seen here. The $p_0(0^+)$ and $p_1'(2^+)$ channels appear to resonate at about $E_p=5.5$ MeV (see Fig. 4) near the estimated $E_x=4.012$ analog position, although the partial waves involved are not obvious from the data.

It is evident from Figs. 2 and 3 that for the less pronounced resonances, there is no strict criterion for deciding which arise from an analog state and which is a background fluctuation. Certainly for the weak states between $E_p=5$–6 MeV, no clean separation seems possible from the present data. In other cases, such as the anomalies at $E_p=6.21$ or 6.58 MeV, the averaged excitation function (Fig. 4) and the correlation of $p_1'(2^+)$ and $p_2'(4^+)$ enhancements with expected positions from $Ti^{50}(d, p)Ti^{51}$ do indicate the presence of a virtual state. Additional data at other angles would be helpful in this connection.

The average Coulomb separation between analog states calculated on the basis of the match made in Table I and in Figs. 3 and 4 were 7702 keV for $2p$, 7739 keV for $1f_{5/2}$, 7737 keV for $2d$, and 7734 keV for $3s_{1/2}$ orbits compared to the value of 7754 ± 30 keV for the Ti^{51} ground-state analog quoted from Sherr.[9]

B. Widths and Spectroscopic Factors

The total width Γ_0 for an analog state was determined here by optimizing the Breit-Wigner fits to the

[8] We have discussed this with the authors of Ref. 4, and upon reexamining their data for this (d, p) transition, they agree that a misinterpretation could have been made.

[9] R. Sherr, Phys. Letters **24**, 321 (1967).

TABLE I. Comparison of the $Ti^{50}(p, p)$ and (p, p') results with those from the $Ti^{50}(d, p)Ti^{51}$ reaction. $E_x' = E_p(\text{c.m.}) - 3.553 + 2.189$, where $E_p(\text{c.m.})$ is the c.m. energy for the resonance and 3.553 MeV is the c.m. energy for the $2p_{3/2}$ analog resonance corresponding to $E_x = 2.189$ MeV in Ti^{51}. Γ_0 is the total width of the state determined by the Breit-Wigner fits to the elastic data or by the observed half-width of the inelastic resonance shape; and Γ_p and $\Gamma_{p'}$ are elastic and inelastic proton escape widths, respectively. The method for determining the spectroscopic factors S_{pp} and $S_{pp'}$ is described in the text. The J^π values indicated are suggested by the data or by simple shell-model considerations and are discussed in Sec. III.

	$Ti^{50}(d,p)Ti^{51}$ [a]			$Ti^{50}+p$ analog states								
Level No.	E_x ±0.008 (MeV)	l_n, j^π	$S_{l,j}$ [b]	E_p (lab) ±0.020 (MeV)	$E_{x'}$ ±0.020 (MeV)	Proton decay channel	l, j^π	Γ_0 (keV)	Γ_p (keV)	$\Gamma_{p'}(2^+)$ (keV)	S_{pp}	$S_{pp'}(2^+)$
0	0.0	$1, \frac{3}{2}$	0.62									
1	1.160	$1, \frac{1}{2}^-$	0.48									
4	2.136	$3, \frac{5}{2}^-$	0.33									
5	2.189	$1, \frac{3}{2}$	0.065	3.620	2.189	$0^+, 2^+$	$1, \frac{3}{2}^-$	33	5.5	7.8	0.078	0.93
				4.170	2.722	$(0^+)2^+$						
6	2.896	$1, (\frac{1}{2}^-)$	0.31				$1, \frac{1}{2}^-$	90	30	19	0.23	0.75
				4.315	2.864	$0^+, 2^+$						
7	3.164	$1, (\frac{3}{2}^-)$	0.088	4.575	3.119	$0^+, 2^+$	$1, \frac{3}{2}^-$	70	16	17	0.11	0.48
8	3.759	4		5.264	3.794	$(0^+), 2^+$	$(3, \frac{5}{2}^-)$	20				
9	4.012	3, (1)	0.052	5.490	4.017	$0^+, (2^+)$		15				
				(5.610)		2^+						
10	4.162	$2, \frac{5}{2}^+$	0.048	5.680	4.173	$0^+, 2^+$	$2, \frac{5}{2}^+$	50	10		0.045	
11	4.460	n.s.		5.910	4.427	$2^+, 4^+$		40				
				6.024	4.539	$2^+, 4^+$		20				
12	4.559	$1, (\frac{3}{2}^-)$	0.025									
				6.057	4.571	$2^+, 4^+$		20				
13	4.592	$2, (\frac{5}{2}^+)$	0.088	6.080	4.594	$0^+, 2^+$	$2, (\frac{5}{2}^+)$	70	7		0.024	
14	4.747	n.s.		6.216	4.727	$(0^+), 2^+, (4^+)$		30				
15	4.810	$0, \frac{1}{2}^+$	0.045	6.325	4.835	2^+		45				
		$0, \frac{1}{2}^+$	0.065 [c]									
16	4.872			6.372	4.880	$0^+, 2^+, 4^+$	$3, \frac{5}{2}^-$	50	16		0.36	
		$3, \frac{5}{2}^+$	0.33									
17	4.988											
		$0, \frac{1}{2}^+$	0.040	6.467	4.973	$2^+, 4^+$		35				
18	5.003											
				6.530	5.035	2^+		30				
19	5.092	?		6.582	5.086	$(0^+), 2^+, (4^+)$		25				
20	5.139	$(3, \frac{5}{2}^-)$ [c]	(0.36) [c]	6.667	5.169	$0^+, 2^+$		40				
21	5.214	?		6.760	5.260	2^+		15				
				6.804	5.303	4^+		20				
				6.930	5.427	$0^+, 2^+, 4^+$	$(2, \frac{5}{2}^+)$	(50)	(10)			
				7.015	5.510	$0^+, 2^+, 4^+$	$(2, \frac{5}{2}^+)$	(40)	(8)			

[a] See Ref. 1.

[b] Calculated from $(2J+1)S_{lnj}$ given in Ref. 1 by using the spin indicated in column 3.

[c] The l_n assignments for level Nos. 16 and 20 of Ref. 1 are discussed in the text and the possibility of a misinterpretation is considered. Our results favor an $l_n = 3$ assignment for level 16 and cast doubt on the l_n character of level 20.

elastic and inelastic resonances seen in the averaged curve of Fig. 4. The elastic width Γ_p is then deduced from the former fits, a few examples of which are shown in Fig. 5. The theoretical curves are calculated with a computer code[10] that employs undistorted Coulomb waves, hard-sphere phase shifts, and no adjustable phase between the background and resonant scattering amplitudes. Because of the residual fine structure (see Sec. III A), the comparison of these calculated curves to the averaged data is sometimes not well defined, with resultant ambiguities in the parameter Γ_p. The procedure seems inadequate to account for small satellite fragments of the large anomalies, e.g., the $E_p=4.15$-MeV $p'(2^+)$ resonance associated with the large 4.3-MeV $2p$ state, and, therefore, points to the need for a more microscopic treatment. The need for the intermediate phase mentioned above is also evident in the fits to the lowest $2p$ and $2d$ states and probably arises from $T_<$ damping of the analog configuration and the presence of coupling to the inelastic channels. A discussion of the problems in extracting $\Gamma_{p'}$ for the $p'(2^+)$ channel is deferred to Sec. III C.

The single-particle spectroscopic factor S_{pp} is given by the relationship

$$S_{pp}{}^{lj}=(2T_0+1)(\Gamma_p{}^{lj}/\Gamma_{sp}{}^{lj}), \qquad (1)$$

where $2T_0=(N-Z)=6$ for Ti^{50} and $\Gamma_{sp}{}^{lj}$ the width of an l, j, single-proton size resonance in a real nuclear well. We have taken $\Gamma_{sp}=2P_l\gamma_{sp}$, where P_l is the penetrability[11] and $\gamma_{sp}=\hbar^2/m_pR_0^2$ with $R_0=1.25A^{1/3}$ is the reduced width. The values of Γ_0, Γ_p, and $S_{pp}{}^{lj}$ are given in Table I. The last quantities are seen to match roughly the values of the spectroscopic factors $S_{dp}{}^{lj}$ determined from $Ti^{50}(d, p)Ti^{51}$ (Ref. 1), although this agreement is moderated by the uncertainties present in the above analysis.

Two qualitative points are worth noting about the analysis of the gross structure just given. The first is that the contributions from incoherent compound elastic and inelastic scattering were neglected here. Some justification for this lies in the fact that we are above the $Ti^{50}(p, n)V^{50}$ threshold[12] ($E_p=3.15$ MeV). A neutron decay of a compound-nucleus state should be highly favored over the charged-particle modes because of the latter's Coulomb barrier, provided that the decay does not require very high angular momentum, i.e., low enough spin states in V^{50} are available. From the increase in yield of the $Ti^{50}(p, n)V^{50}$ reaction[12] above $E_p=3.5$ MeV and (He^3, d) data on the level structure of V^{50} (Ref. 13), this condition seems to be met in our experiment.

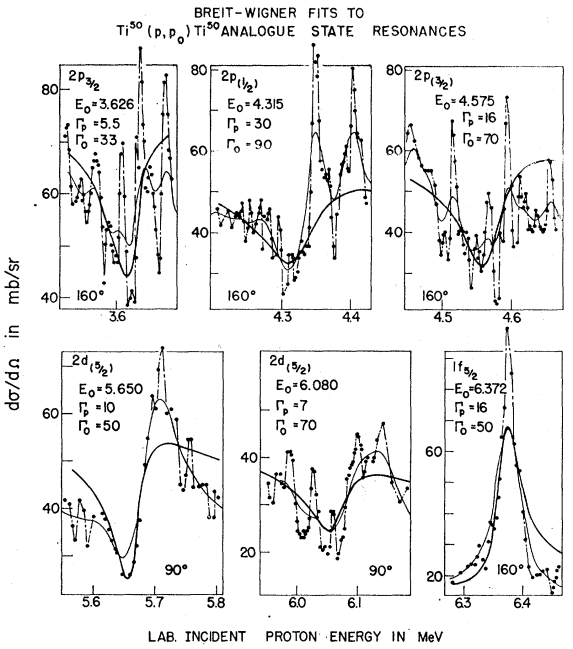

FIG. 5. Some comparisons of calculated Breit-Wigner shapes and the analog resonance results. The points lie on the dashed line drawn through the experimental data shown in Figs. 2 and 3 and are thus interpolated between data points. The light solid line represents an average of the data that was shown in Fig. 4. The heavy solid curves are the theoretical resonance shapes calculated with a code that utilizes only a hard sphere and Coulomb phase between the potential and resonant scattering amplitudes. It is evident from the quality of the comparison that an additional intermediate phase is necessary to reproduce the high-low energy asymmetries of the resonant shapes and that residual fine-structure effects would preclude a close fit to the over-all analog-state anomaly.

Second, the large $p'(2^+)$ enhancements at 4.3 and 4.6 MeV in Fig. 2 appear to have slightly asymmetric shapes characterized by low-energy tails. Such asymmetries have been explained by several authors[14,15] for the case of one open proton channel, and we gather that a similar feature would carry over for many open reaction channels. They arise from an interference between the pure analog resonance and the non-negligible direct-escape amplitudes of the certain $T_<$ states, possibly other doorway states or neighboring antianalog fragments. One consequence is that, in properly parametrizing the shapes in the average elastic cross sections, say, to obtain a spectroscopic factor, some knowledge of these interfering terms (or equivalently the analog-state spreading and the background optical absorption must be available.

[10] N. A. Brown, T. A. Belote, and R. R. Perry (unpublished). Code based on the formalism of J. M. Blatt and L. C. Biedenharn, Rev. Mod. Phys. **24**, 155 (1952).

[11] H. Feshbach, M. M. Shapiro, and V. F. Weisskopf, Atomic Energy Commission Technical Report No. NYO-3077, 1953 (unpublished).

[12] G. J. McCallum, A. T. G. Ferguson, and G. S. Mani, Nucl. Phys. **17**, 116 (1960).

[13] J. N. Bishop, D. J. Pullen, and B. Rosener, University of Pennsylvania Tandem Accelerator Progress Report, 1967 (unpublished).

[14] D. Robson, Phys. Rev. **137**, B535 (1965); C. Mahaux and H. A. Weidenmüller, Nucl. Phys. **A94**, 1 (1967).

[15] A. K. Kerman and A. F. R. de Toledo Piza, Ann. Phys. (N.Y.) **48**, 173 (1968).

A detailed width analysis of the fine structure would also have been desirable here, but there were several aspects of the data that precluded it. In the elastic excitation function, Figs. 2 and 3, it is evident that considerable fluctuations exist and obscure any narrow shapes. Furthermore, because of the open (p, p') and (p, n) channels, the widths are approaching the size of the spacings for the fine-structure resonances, and the elastic interference patterns become unmanageably complex. The situation is less severe in the inelastic case where individual states, full widths, and peak heights are discernible. However, without additional information on the elastic or (p, n) channels, these are not enough to determine partial widths which would be of interest in theoretical analysis of strength functions and sum rules.

C. Inelastic Scattering

The inelastic proton decay of an analog resonance can, in principle, reveal spectroscopic information on the parent state in the neighboring isobar which is often not obtainable by any other reaction. In particular, knowledge of the associated partial widths can determine directly the particle-hole or core-excited character of the state in question. In many cases, however, the reaction process involved is not well understood, and reliable values for these widths become difficult to extract. In this section, we discuss qualitatively the nuclear-structure information on Ti^{51} suggested by the $p_1'(2^+)$ and $p_2'(4^+)$ data and some of the difficulties that seem to prevent a clear analysis of the results.

In a previous paper, the $Sr^{88}(p, p')$ enhancements were explained in terms of four different reaction processes, and here we shall adopt the same type of approach for the $Ti^{50}(p, p')$ case. According to process I, a (p, p') resonance is generated via a direct parentage in the sense of the core-excited model of the Ti^{50} state corresponding to the analog state in question and the excited states of Ti^{50}. Suppose, for example, that the $2p_{3/2}$ state in Ti^{51} at $E_x=2.189$ MeV is a mixture of $(p_{3/2})_n\phi_0$ and $[(p_{3/2})_n\phi_{2^+}]_{3/2}$ components, where ϕ_0 and ϕ_{2^+} are the ground and first 2^+ states in Ti^{50}. Then, the analog of these terms would couple strongly to and produce resonances in the $p_0(0^+)$ and $p_1(2^+)$ channels, respectively. Process II requires an overlap of the analog state and neutron particle-hole configurations in Ti^{50}. For instance, the analog of the first term in the above example, $T^-[(p_{3/2})_n\phi_0]$, will contain a term $(p_{3/2})_n[(f_{7/2})_p{}^3(f_{7/2})_n{}^{-1}]_{J=0}$ which will decay by simple $f_{7/2}$ proton emission to ϕ_{2^+} if this wave function contains an appreciable $[(p_{3/2})_n(f_{7/2})_n{}^{-1}]_{2^+}$ component. In process III, the direct nuclear and Coulomb (p, p') transition amplitudes are enhanced on resonance through the coupling of the incident and/or exit continuum waves to the analog state. Such a process might arise from the existence of a pronounced elastic resonance only; however, if processes I and II are also present, it may interfere with them and produce anomalous scattering angular distributions. Finally, there is the compound inelastic scattering process IV. This proceeds through the $T_<$ normal states in V^{51} and undergoes a resonance by their coupling to the analog doorway configuration. If this is incoherent, the branching ratios for compound nucleus should be governed only by penetrabilities, and, therefore, the p' modes should be strongly diminished in the presence of open neutron channels. However, if the normal states themselves have significant coupling to the continuum, e.g., via other doorways, interference effects might be expected.

The most prominent $p_1'(2^+)$ resonances are associated with the $2p$ analog states at $E_p=3.6$, 4.3, and 4.6 MeV and can be reasonably explained by the core-excited model. In this picture, one expects strong fragments of the $[(p_{3/2})_n\phi_0]_{3/2^-}$ and $[(p_{1/2})_n\phi_0]_{1/2^-}$ configurations in Ti^{51} at low excitations in agreement with the two strong $l_n=1$ states seen in $Ti^{50}(d, p)Ti^{51}$ (Ref. 1) at $E_x=0.0$ and 1.160 MeV with $S(\frac{3}{2}^-)=0.62$ and $S(\frac{1}{2}^-)=0.48$, respectively. Furthermore, these configurations should mix with $[(p_{3/2})_n\phi_{2^+}]_{3/2^-}$, $[(p_{3/2})_n\phi_{2^+}]_{1/2^-}$, and $[(p_{1/2})_n\phi_{2^+}]_{3/2^-}$ occurring from $E_x=2$–3 MeV producing the three isolated $l_n=1$ levels at $E_x=2.136$, 2.896, and 3.164 MeV that correspond to the analogs mentioned above. Thus, the picture is consistent with the strong 2^+ decays observed here and suggests that they have dominant contributions from process I. Process II, on the other hand, should be negligible, since it is known from $Ti^{49}(d, p)Ti^{50}$ (Ref. 2) that ϕ_{2^+} contains less than 5% admixture of $(f_{7/2})_n{}^{-1}(p_{3/2})_n\phi_0$ and in addition that the requisite $l_p=3$ proton emission is suppressed relative to $l_p=1$ by the angular momentum barrier.

The angular distributions taken over these resonances are shown in Fig. 6 and provide further evidence on the mechanisms and spins involved. On the largest fragments of the lowest resonance ($E_1=3.612$ and $E_2=3.632$ MeV), the shapes were symmetric about $\theta=90°$ and are matched well by the function $W(\theta)=1-0.6P_2(\theta)$ which is the predicted pattern[16] assuming an intermediate spin of $J_0{}^\pi=\frac{3}{2}^-$ and incident and exit angular momenta of $J_{\text{in}}{}^\pi=\frac{3}{2}^-$ and $J_{\text{out}}{}^\pi=\frac{3}{2}^-$. Thus, the parent level in Ti^{51} at 2.189 MeV should contain a large $[(p_{3/2})_n\phi_{2^+}]_{3/2^-}$ amplitude. The off-resonance distribution at $E_3=3.855$ MeV is low and flat, characteristic of a predominately compound-nucleus background. The exposures taken on the upper two $2p$ resonances at $E_{4,5,6}\geq 4$ MeV all show distinct asymmetries which point to a direct interference from process III. This is not a function of the particular fine-structure peak considered, since the patterns at E_4 and E_5 on two well-separated fragments of the 4.3-MeV anomaly are

[16] E. Sheldon and D. M. Van Patter, Rev. Mod. Phys. **28**, 143 (1966).

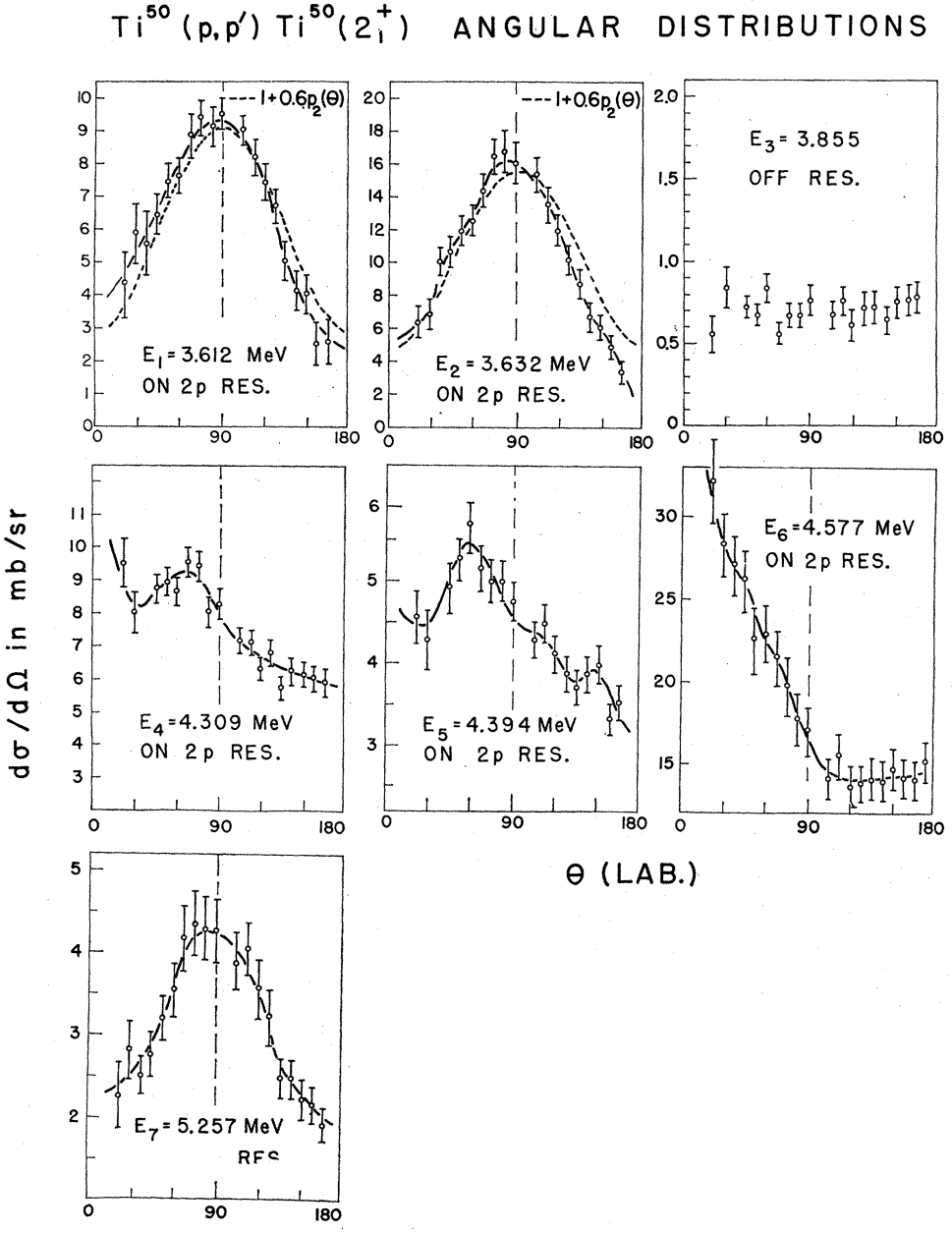

FIG. 6. The $Ti^{50}(p, p')$ angular distributions for the 2^+ (1.555-MeV) transition. The solid lines drawn through the data points are there merely as visual guidelines. The dashed curves, included in some cases, represent sums of Legendre polynomials and have been used to infer spins of the corresponding analog state. In several cases, the distributions show considerable structure and pronounced asymmetries about 90°.

identical. We note that, although the Coulomb (or nuclear) excitation background is estimated[17] to be ≤ 0.025 mb/sr at $E_p = 4$ MeV, it may be sufficiently enhanced on resonance by increased penetration of the continuum waves to be responsible for this effect. Clearly, this anomalous behavior would preclude any simple spin determination for the upper two $2p$ states.

The inelastic width $\Gamma_{p'}$ on the lowest $2p$ analog was determined by the relationship

$$\sigma_{max} = 2\pi\lambda^2(2J_0+1)(\Gamma_p\Gamma_{p'}/\Gamma_0^2), \qquad (2)$$

where σ_{max} is the total on-resonance cross section for

[17] K. Alder, A. Bohr, T. Huus, B. Mottelson, and A. Winther, Rev. Mod. Phys. **28**, 432 (1956).

the averaged data of Fig. 4, and Γ_p and Γ_0 are the widths found in Sec. III B. The corresponding spectroscopic factor S_{pp} is calculated by Eq. (1), and the implied wave function for the parent state at $E_x=2.189$ MeV in Ti^{51} becomes

$$\psi_{3/2^-}(2.189)=(S_{pp})^{1/2}[(p_{3/2})_n\phi_0]_{3/2^-}+(S_{pp'})^{1/2}[(p_{3/2})_n\phi_{2^+}]_{3/2^-} \quad (3)$$

with $S_{pp}=0.08$ and $S_{pp'}=0.93$.

In order to estimate crudely the contribution from process I for the upper $2p$ resonances, we have assumed that the direct effects are smallest at the back angles and used the data there to extrapolate a value of $\sigma_{\max}$ in Eq. (2). $\Gamma_{p'}$ is still undefined since J_0 is not known. However, the choice of $\frac{1}{2}^-$ and $\frac{3}{2}^-$ for the $E_x=2.896$- and 3.164-MeV states in Ti^{51} produces better agreement between present S_{pp} values and the $S^{l,j}$'s from the (d, p) experiment and therefore is favored by our analysis. Table I summarizes the values of $\Gamma_{p'}$ and $S_{pp'}$ found here. The determination of the quantities for other resonances and transitions was not attempted, since the angular distributions were not measured, and therefore the partial waves involved would at best be speculative.

The fragmentation of the $1f_{5/2}$ single-particle states below $E_x=5$ MeV in Ti^{51} might also be interpreted as mixing with configurations involving $2p$ or $1f_{5/2}$ particles coupled to the first 2^+ or 4^+ states in Ti^{50}. This is consistent with our data where the largest observed $l=3$ elastic anomaly at $E_p=6.4$ MeV is accompanied by a pronounced 2^+ peak (see Fig. 2) and a weak 4^+ resonance, both presumably going by process I. Again the $Ti^{49}(d, p)Ti^{50}$ results rule out process II. As discussed in Sec. III A, the $p'(2^+)$ bump at $E_p=5.25$ MeV could be the analog of the $E_x=4.012$-MeV, $J^\pi=\frac{5}{2}^-$ state, even though it is closer to the expected position for a $g_{9/2}$ analog level. The corresponding angular distribution in Fig. 6 supports this possibility, since its shape resembles that of an intermediate-state process with $J_{\text{in}}{}^\pi=\frac{5}{2}^-$, $J_0{}^\pi=\frac{5}{2}^-$, and $J_{\text{out}}{}^\pi=\frac{3}{2}^-$, but is dissimilar to any transition involving $J_0{}^\pi=\frac{9}{2}^+$. The latter may not be detectable here because of the very low penetrability for an incident angular momentum of $l=4$.

The positive-parity $2d$ and $3s_{1/2}$ states are typically highly fragmented and spread out in energy. In our experiment, we see indications in Figs. 3 and 4 of the analogs to the lowest five such states identified in the $Ti^{50}(d, p)Ti^{51}$ reaction and possibly several others at a slightly higher energy. These states account for only a small fraction of the total strength and the remainder is beyond the range covered here. If the matching suggested in Fig. 4 and Table I is correct, these virtual levels appear to decay favorably to the 2^+ state and thus may have components of the type $[(2d)_n\phi_{2^+}]_J$ and $[(s_{1/2})_n\phi_{2^+}]_J$. The observed $J_0{}^\pi=\frac{1}{2}^+$ states should not decay to the 4^+ level since the only appropriate term with which to mix, $[(1g_{9/2})_n\phi_{4^+}]_{1/2^+}$, is distant in energy. The $3s_{1/2}$ analog at 6.34 MeV indeed does not exhibit a 4^+ decay, and the fact that a weak 4^+ peak is seen on the 6.47-MeV doublet indicated that one of these states is not an $l=0$. The lowest two $2d_{5/2}$ analogs at $E_p=5.67$ and 6.08 MeV also do not resonate to the 4^+ state, which is understandable again by the remote position of the $[(2d_{5/2})_n\phi_{4^+}]_J$ energies in the parent nucleus. At an excitation of about 1.5 MeV higher, however, we detected two levels $E_p=6.96$ and 7.05 MeV that display tentatively weak $l=2$ patterns in the elastic scattering and resonate both in the 2^+ and 4^+ channels. They presumably then correspond to $\frac{5}{2}^+$ or $\frac{3}{2}^+$ states in Ti^{51} built from combinations of the $2d$ neutrons coupled to ϕ_{0^+}, ϕ_{2^+}, and ϕ_{4^+}.

Numerous less pronounced $p_1'(2^+)$ and $p_2'(4^+)$ resonances are evident here where no associated elastic disturbance is discernible. Some of these correspond to the nonstripping levels observed in the $Ti^{50}(d, p)Ti^{51}$ experiment, and others appear to have no match with previously known states. They undoubtedly are analogs to nonsingle-particle configurations, such as $[(p_{3/2})_n\phi_{2^+}]_{J^\pi}$ and $[(p_{3/2})_n\phi_{4^+}]_{J^\pi}$ with $J^\pi\geq\frac{7}{2}^-$ whose entrance elastic widths arise from a weaker compound-nucleus mechanism.

At energies beginning above $E_p=6$ or 7 MeV, one would expect to see enhanced transitions to odd-parity collective states or to the positive-parity particle hole and possibly deformed levels at $E_x>4$ MeV in Ti^{50}. An interesting case is the inelastic resonances to the first 3^- at $E_x=4.38$ MeV which should arise from the mixing of the $2d$, $3s_{1/2}$, and $1g_{7/2}$ states with configurations, such as $[(2p)_n\phi_{3^-}]_J$ and $[(1f_{5/2})_n\phi_{3^-}]_J$ in Ti^{51}. The strength of the former single-particle states is predicted to be dissipated over several MeV and to show weakly in the elastic scattering, however, the latter's strength should be much less dispersed[18] in energy and be enhanced as an exit-channel (p, p') resonance because of the collectivity of the octupole state. Unfortunately, the 3^- proton group was obscured by C^{13} contaminant peaks in the back angles over the relevant range studied here. However, at higher energies, this difficulty would be removed and such an extension of the present experiment would be of interest in providing further tests of the core-excited model.

IV. CONCLUSIONS

A potentially large amount of nuclear-structure information in this mass region can be derived from the present type of data, especially the inelastic scattering. Complete (p, p') angular distributions are particularly important not only for performing partial-wave analyses and determining spins, but also for revealing the importance of direct interference effects that can be sizable and obscure the simple results. The spectro-

[18] N. Stein, C. A. Whitten, and D. A. Bromley, Phys. Rev. Letters 20, 113 (1967).

scopic information from the elastic scattering is consistent with previous (d, p) data and the inelastic transitions can be successfully explained by a core-excited picture for the low-lying levels of Ti^{51}. Similar studies at higher energies examining the transitions to the collective states above 4 MeV in Ti^{50} should be of interest and perhaps provide more stringent tests of the weak-coupling model.

ACKNOWLEDGMENTS

The authors wish to thank Professor H. Feshbach and Professor A. K. Kerman for their stimulating interest in the present work. The encouragement of Professor W. W. Buechner and Professor H. A. Enge is also greatly appreciated. We thank Mrs. Claire Pritchard for her careful scanning of the nuclear emulsions and Mrs. Mary E. White for preparing the manuscript.

PHYSICAL REVIEW VOLUME 182, NUMBER 4 20 JUNE 1969

Excitation of the $\frac{3}{2}^+$, 2.02-MeV State in ^{41}Ca by the (t, d) Reaction*

G. R. SATCHLER
Oak Ridge National Laboratory, Oak Ridge, Tennessee 37830
AND
D. D. ARMSTRONG, A. G. BLAIR, AND E. R. FLYNN
Los Alamos Scientific Laboratory, Los Alamos, New Mexico 87544
AND
R. J. PHILPOTT† AND W. T. PINKSTON
Vanderbilt University, Nashville, Tennessee 37203

(Received 7 February 1969)

The ^{40}Ca (t, d) reaction, with 20-MeV tritons, was used to excite the ground and first two excited states of ^{41}Ca. The measured differential cross sections were analyzed using the distorted-wave method, assuming the usual first-order stripping mechanism. The triton optical potential was obtained by fitting measurements of the elastic scattering. The spectroscopic factor C^2S for $d_{3/2}$ capture into the 2.02-MeV state was found to be about 0.06 times that for $f_{7/2}$ capture into the ground state when the usual well-depth prescription was used for the neutron wave function. More realistic $d_{3/2}$ neutron form factors based upon simple model wave functions for ^{40}Ca and ^{41}Ca were also used. They led to spectroscopic factors which are at least twice as large and are found to be very sensitive to the type of nucleon-nucleon interaction assumed. The implications for the amount of particle-hole excitation in the ground state of ^{40}Ca are discussed.

I. INTRODUCTION

THERE is considerable interest in the information on the departure of the ^{40}Ca ground state from a doubly closed shell configuration which can be obtained from nucleon transfer reactions. For example, by studying nucleon capture transitions to states in the $A=41$ residual nuclei which have predominantly two-particle one-hole configurations, one can hope to learn something about the amount of two-particle two-hole mixtures in the ^{40}Ca ground state. In particular, excitation of the $\frac{3}{2}^+$ level at 2.02 MeV in ^{41}Ca by simple neutron transfer to ^{40}Ca depends upon the amount of $(d_{3/2}^{-2}, j^2)$ admixture present in the target if this residual state has a configuration of the type $(d_{3/2}^{-1}, j^2)$. Of course, such a measurement only places a lower limit on such admixtures. If, as we expect, the states contain contributions from several such configurations, the total strength will be distributed amongst several $\frac{3}{2}^+$ final states in ^{41}Ca.

Several measurements of the excitation of this state by the $^{40}Ca(d, p)^{41}Ca$ reaction have been reported[1] and distorted-wave analyses have yielded spectroscopic factors C^2S with values between 0.05 and 0.20. Now $4\Sigma(C^2S)$, where Σ is the sum over the various $\frac{3}{2}^+$ final states in ^{41}Ca, is equal to the number of $d_{3/2}$ neutron holes in the ^{40}Ca ground state. Hence, the 2.02-MeV level appeared to contribute between 0.2 and 0.8 to this sum.

In all these analyses, the well-depth prescription was used to construct the form factor[2] for the captured neutron. That is to say, it was taken to be the wave function for a $1d_{3/2}$ neutron moving in a Woods-Saxon

* Research jointly sponsored by the U.S. Atomic Energy Commission and by the U.S. National Science Foundation.

† Present address: Florida State University, Tallahassee, Fla. 32306.

[1] T. A. Belote, A. Sperduto, and W. W. Buechner, Phys. Rev 139, B80 (1965); A. Denning, J. G. B. Haigh, and G. Brown, Phys. Letters 27B, 159 (1968); T. A. Belote, W. E. Dorenbusch, and J. Rapaport, Nucl. Phys. A120, 401 (1968); K. K. Seth, J. Picard, and G. Bassani (unpublished).

[2] R. J. Philpott, W. T. Pinkston, and G. R. Satchler, Nucl. Phys. A119, 241 (1968).